BIOCHEMISTRY
including biophysical chemistry & molecular biology

Article

pubs.acs.org/biochemistry

# Conformational Differences between the Methoxy Groups of $Q_A$ and $Q_B$ Site Ubisemiquinones in Bacterial Reaction Centers: A Key Role for Methoxy Group Orientation in Modulating Ubiquinone Redox Potential

Alexander T. Taguchi,[†] Patrick J. O'Malley,*[,∥] Colin A. Wraight,*[,†,§] and Sergei A. Dikanov*[,‡]

[†]Center for Biophysics and Computational Biology, [§]Department of Biochemistry, and [‡]Department of Veterinary Clinical Medicine, University of Illinois at Urbana−Champaign, Urbana, Illinois 61801, United States

[∥]School of Chemistry, The University of Manchester, Manchester M13 9PL, U.K.

Supporting Information

**ABSTRACT:** Ubiquinone is an almost universal, membrane-associated redox mediator. Its ability to accept either one or two electrons allows it to function in critical roles in biological electron transport. The redox properties of ubiquinone *in vivo* are determined by its environment in the binding sites of proteins and by the dihedral angle of each methoxy group relative to the ring plane. This is an attribute unique to ubiquinone among natural quinones and could account for its widespread function with many different redox complexes. In this work, we use the photosynthetic reaction center as a model system for understanding the role of methoxy conformations in determining the redox potential of the ubiquinone/semiquinone couple. Despite the abundance of X-ray crystal structures for the reaction center, quinone site resolution has thus far been too low to provide a reliable measure of the methoxy dihedral angles of the primary and secondary quinones, $Q_A$ and $Q_B$. We performed 2D ESEEM (HYSCORE) on isolated reaction centers with ubiquinones $^{13}$C-labeled at the headgroup methyl and methoxy substituents, and have measured the $^{13}$C isotropic and anisotropic components of the hyperfine tensors. Hyperfine couplings were compared to those derived by DFT calculations as a function of methoxy torsional angle allowing estimation of the methoxy dihedral angles for the semiquinones in the $Q_A$ and $Q_B$ sites. Based on this analysis, the orientation of the 2-methoxy groups are distinct in the two sites, with $Q_B$ more out of plane by 20−25°. This corresponds to an ≈50 meV larger electron affinity for the $Q_B$ quinone, indicating a substantial contribution to the experimental difference in redox potentials (60−75 mV) of the two quinones. The methods developed here can be readily extended to ubiquinone-binding sites in other protein complexes.

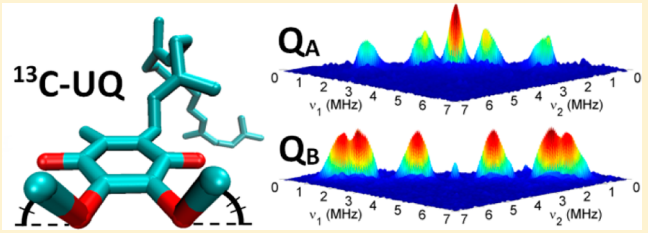


The reaction center (RC) of the photosynthetic bacterium, *Rhodobacter (Rb.) sphaeroides*, is an integral membrane protein that separates charge upon photoactivation with ∼100% quantum yield.[1,2] Light activation causes transfer of an electron from a pair of bacteriochlorophylls to a ubiquinone-10 (UQ-10) occupying the $Q_A$ site on the other side of the membrane, forming the semiquinone anion radical, $SQ_A$. $SQ_A$ can then transfer its electron to another, chemically identical, UQ-10 in the $Q_B$ site, forming $SQ_B$.[3,4] Passage of the electron from $SQ_A$ to $Q_B$ is essential to allow further photochemical turnover of the RC, and is energetically favorable in spite of the chemical identity of $Q_A$ and $Q_B$. The redox potential of $Q_B$ is 60−75 mV more positive than $Q_A$.[5−9] The origin of this redox potential difference is not yet known, but only quinones with methoxy groups are able to serve as $Q_A$ and $Q_B$ simultaneously.[10,11] Furthermore, experiments with monomethoxy ubiquinone-4 analogs show that simultaneous function as $Q_A$ and $Q_B$ specifically requires only the 2-methoxy group[10] suggesting that this group is somehow involved in generating the necessary difference in redox potential between $Q_A$ and $Q_B$. The methoxy groups not only have an impact on the redox potential of the quinone and resultant catalytic activity,[12,13] but may also contribute to interactions necessary for correct and adequate binding, especially for $Q_B$.[10] Thus, a role for the methoxy groups is indicated that suggests protein-imposed constraints on the dihedral angle of the methoxy groups of UQ in their respective sites. This has clear implications for the much wider involvement of ubiquinones in key membrane redox function.

The plethora of X-ray structures now available does not provide an unequivocal description of the two quinone sites in the RC, which are positioned almost symmetrically about a central $Fe(His)_4$ complex. The H-bond distances and the torsional angles of the two methoxy group substituents of the ubiquinone ring display a significant spread in different structures, indicating mobility or mosaicity (reviewed in ref 4). However, for $Q_B$ in the proximal position relative to the $Fe(His)_4$ center, the majority of structures yield a consensus

**Received:** April 18, 2013
**Published:** June 9, 2013

   dx.doi.org/10.1021/bi400489b | *Biochemistry* 2013, 52, 4648−4655

with both methoxy groups strongly out of plane. This is superficially similar to the average conformation for $Q_A$, except 180° out of phase.[4] Alternative approaches to obtaining these geometric parameters are spectroscopy and computation. Vibrational spectroscopy, and FTIR spectroscopy, in particular, provide significant and independent insights to the quinone binding interactions,[4,14] while EPR methods have been applied with great effect to the semiquinone states.[15,16] An advantage of IR and Raman over magnetic resonance spectroscopies is that the former, by difference spectroscopy, can see all redox states of the quinones, not just the radical species. The use of light-induced (or redox potential-induced) difference spectra has allowed resolution of the difference between quinone and SQ states in RCs (for reviews, see refs 13, 17). The theoretical and experimental bases for the IR spectra of ubiquinones, in solution, have been systematically explored.[18−23] The observation of two C═O stretches indicates asymmetry of substitution, arising from the conformations of the two methoxy groups, since an in-plane methoxy donates electrons into the ring while those out of plane are electron withdrawing. In addition, the influence of methoxy group conformations on transition energies and electron affinity have been quantum-chemically calculated for model quinones and ubiquinones.[19,21,24−26]

$Q_A^-$−$Q_A$ and $Q_B^-$−$Q_B$ IR difference spectra, including spectra of UQ-10 site-specifically $^{13}$C-labeled at the C2 and C3 positions (see Scheme 1 for numbering convention) and

**Scheme 1**

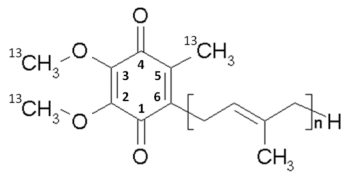

reconstituted to either the $Q_A$ or the $Q_B$ binding site, were used to study the inequivalence of the methoxy groups.[27] The spectra did not show a shift in frequency of (ring)C−O vibrations at either the $Q_A$ or $Q_B$ binding sites, as compared with unbound UQ-10. On this basis, it was concluded that the methoxy groups are similarly oriented out of plane in both sites and do not contribute significantly to the differences of redox energies between $Q_A$ and $Q_B$.[27] This is at odds with the functional observations described above, and one can suggest that the necessary redox potential difference is quite small[5−9] and might not result in significant IR spectroscopic changes.

Considering specifically the SQ states in the $Q_A$ and $Q_B$ sites, one can anticipate that orientations of the methoxy substituents can be inferred from analysis of the hyperfine tensor of $^{13}$C labeled methoxy groups as described recently for the SQ in the high-affinity site of cytochrome $bo_3$ ubiquinol oxidase from *E. coli*.[28] At present, no information about $^{13}$C hyperfine couplings in methoxy groups of $SQ_A$ and $SQ_B$ in RCs is available.

In this work, we report the experimental $^{13}$C hyperfine couplings for the methyl and two methoxy groups of $^{13}$C site-specifically labeled $SQ_A$ and $SQ_B$ in RCs of *Rb. sphaeroides*, determined using 2D ESEEM (HYSCORE). Analysis of the couplings to characterize the distribution of the unpaired spin density and conformations of methoxy groups and their influence on the redox properties of the two sites is performed with the aid of DFT calculations of hyperfine tensors and electron affinity values.

## EXPERIMENTAL SECTION

**Samples.** Headgroup $^{13}$C-methyl labeled ubiquinone was biosynthesized in a strain of *E. coli*[29] that is auxotrophic for eight amino acids, including methionine, which is the methyl donor in ubiquinone synthesis. Growth of this strain in the presence of $^{13}$C-methyl methionine results in $^{13}$C labeling of the methoxy and methyl carbons of the ubiquinone headgroup (Scheme 1). The product of biosynthesis in *E. coli* is UQ-8, rather than UQ-10, but no functional differences exist between them.[11]

After growth, ubiquinone was extracted in organic solvents and purified by TLC.[28]

Reaction centers used in this study were isolated from a strain of *Rb. sphaeroides* expressing RCs with a histidine-tag on the M subunit.[30] Cells were grown using $^{15}$N-labeled ammonium sulfate (Cambridge Isotopes), to prevent peak overlap and the strong cross-suppression effects of $^{14}$N on the $^{13}$C modulation.[31] In order to isolate SQ EPR signals, the native, high spin $Fe^{2+}$ must be replaced by diamagnetic $Zn^{2+}$. Procedures for biochemical metal exchange, along with the methods of bacterial cell growth and RC isolation, were as previously described.[32] Quinones were extracted from RCs by the method of Okamura et al.,[33] and were replaced with the $^{13}$C-methyl labeled ubiquinones. The $SQ_A$ radical was generated by dithionite reduction in semianaerobic conditions (with continuous argon flow over the sample). $SQ_B$ was generated by exposing the RCs to a single 532 nm Nd:YAG laser pulse in the presence of ferrocytochrome *c* (to quickly rereduce the bacteriochlorophyll dimer after charge separation).[32] All samples were frozen promptly in liquid nitrogen. $^{13}$C-labeling of the methyls does not influence the SQ line width, indicating that it is still dominated by the g-tensor anisotropy. The $^1$H, $^{15}$N ESEEM for UQ-8 SQs was identical to the spectra of natural UQ-10 SQs, thus confirming similar H-bond patterns after replacement.

**EPR and ESEEM Measurements.** The CW EPR measurements were performed on an X-band Varian EPR-E122 spectrometer. The pulsed EPR experiments were carried out using an X-band Bruker ELEXSYS E580 spectrometer equipped with an Oxford CF 935 cryostat. All measurements were made at 80 K. The 2D, four-pulse experiment ($\pi/2$-$\tau$-$\pi/2$-$t_1$-$\pi$-$t_2$-$\pi/2$-$\tau$-*echo*, also called HYSCORE),[34] was employed with appropriate phase-cycling schemes to eliminate unwanted features from the experimental echo envelopes. The intensity of the echo after the fourth pulse was measured with $t_2$ and $t_1$ varied and constant $\tau$. The length of a $\pi/2$ pulse was 16 ns and a $\pi$ pulse 32 ns. HYSCORE data were collected in the form of 2D time-domain patterns containing 256 × 256 points with steps of 20 or 32 ns. Spectral processing of ESEEM patterns, including subtraction of the relaxation decay (fitting by polynomials of 3−6 degree), apodization (Hamming window), zero filling, and fast Fourier transformation (FT), were performed using Bruker WIN-EPR V2.22 Rev. 10. Processed data were then imported into Matlab R2010a via the EasySpin package[35] to either be simulated by EasySpin, or be analyzed by a homemade script for fitting data in $(\nu_1)^2$ vs $(\nu_2)^2$ coordinates. After plotting the HYSCORE as $(\nu_1)^2$ vs $(\nu_2)^2$, ridges were fit via a linear regression with each point on the ridge weighted according to its HYSCORE intensity (see below).


dx.doi.org/10.1021/bi400489b | *Biochemistry* 2013, 52, 4648−4655

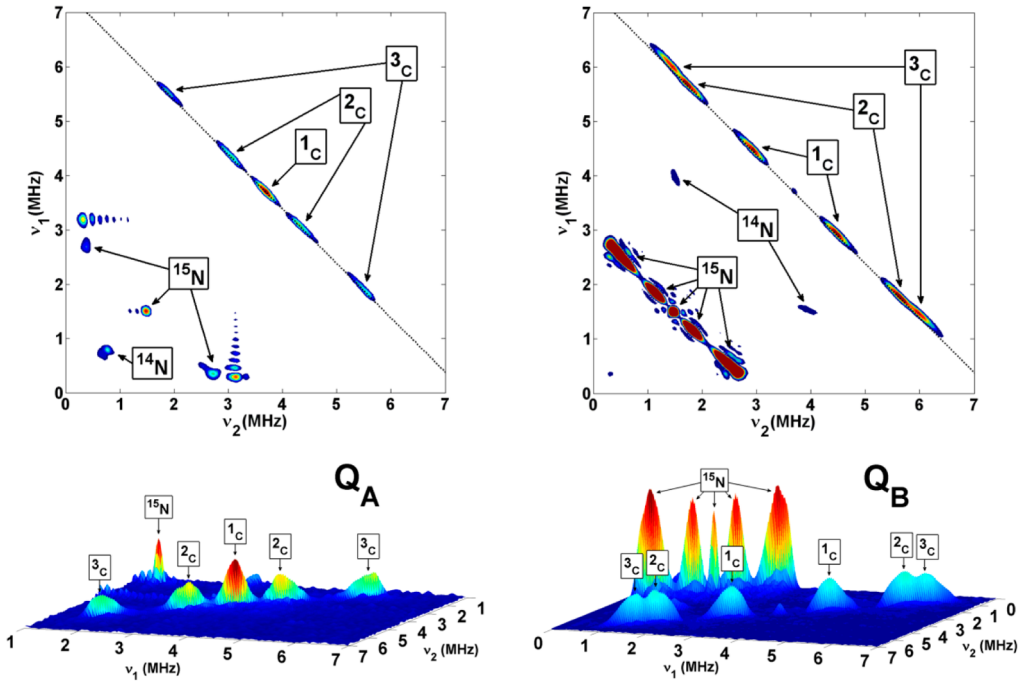


**Figure 1.** Contour (top) and stacked (bottom) HYSCORE spectra of $SQ_A$ (left) and $SQ_B$ (right) in $^{15}N$ uniformly labeled RCs [magnetic field 345.2 mT ($Q_A$) and 345.1 mT ($Q_B$), time between first and second pulses ($\tau$) 136 ns, microwave frequency 9.686 GHz ($Q_A$), and 9.684 GHz ($Q_B$)].

**Computational Methods.** All density functional calculations were performed using Gaussian 09.[36] All calculations, including geometry optimization, conformational analysis, and hyperfine coupling, were performed using the B3LYP functional and the EPR-II basis set. Specific details concerning hyperfine coupling calculations and the $SQ_A$ and $SQ_B$ site models are as previously described.[37−39] In addition to these, two new models of ubisemiquinone were used, termed $SQ_{M1}$ and $SQ_{M2}$. These are shown in Figure S1 of Supporting Information and were used to model the semiquinone hydrogen bonding to four water molecules ($SQ_{M1}$) and one water molecule ($SQ_{M2}$). Conformational analysis using the $SQ_{M2}$ model was achieved by varying the $C_mO_mC2C1$ dihedral angle from 0° to 180° in 20° steps while optimizing all other parameters.

**Powder $^{13}C$ ESEEM Spectra.** The high-resolution pulsed EPR techniques, such as ESEEM and ENDOR, make use of the paramagnetic properties of the SQ intermediate, its interactions with nearby magnetic nuclei of the protein, the aqueous solvent, and the quinone molecule itself. 1D and 2D ESEEM can be used to explore the fine-tuning of the environment, and the geometry of substituents and electronic structure of the SQ, via the isotropic and anisotropic hyperfine interactions with magnetic nuclei ($^{13}C$ in this work).[15] ESEEM measures frequencies of nuclear transitions from nuclei interacting with an $S = 1/2$ electron spin of the SQ. There are only two transitions with frequencies $\nu_\alpha$ and $\nu_\beta$ for $^{13}C$ with nuclear spin $I = 1/2$, corresponding to two different states $m_s = \pm 1/2$ of the SQ electron spin in a constant applied magnetic field. The value of the frequencies depends on the vector sum of the applied magnetic field and local magnetic field induced at the nucleus by the isotropic and anisotropic hyperfine interactions with the electron spin. In this work we used X-band EPR with microwave frequency ∼9.7 GHz and magnetic field ∼350 mT. The X-band EPR spectrum of the SQ in frozen solutions is a single line with the width ∼0.8−1.0 mT with unresolved hyperfine structure. This width is comparable to the excitation width of the EPR spectrum by microwave pulses. In this case, the pulses can be considered as giving a complete excitation of the powder EPR spectrum, and thus the ESEEM spectra obtained are the powder-type spectra of nuclear frequencies with all different orientations of the applied magnetic field relative to the principal axes of $^{13}C$ hyperfine tensor(s). The frequencies of $\nu_\alpha$ and $\nu_\beta$ transitions vary between

$$\nu_{\alpha(\beta)\perp} = |\nu_C + (-) A_\perp/2|$$

and

$$\nu_{\alpha(\beta)\parallel} = |\nu_C + (-) A_\parallel/2| \quad (1)$$

corresponding to the perpendicular and parallel orientations of the magnetic field and the unique axis of the axial hyperfine tensor ($\nu_C$ is the Zeeman frequency of $^{13}C$ in the applied magnetic field, $A_\perp = |a-T|$ and $A_\parallel = |a+2T|$, $a$ is the isotropic hyperfine constant, and the $T$-components of the anisotropic hyperfine tensor are $(-T, -T, 2T)$). The principal values of the rhombic hyperfine tensor can be defined as follows: $(-T(1 + \delta), -T(1 - \delta), 2T)$ with $0 \le \delta \le 1$, where $\delta$ is a rhombic parameter.

In this work we used HYSCORE because it provides better resolution of the extended lines of low intensity. The HYSCORE experiment creates off-diagonal cross-peaks ($\nu_\alpha$, $\nu_\beta$) and ($\nu_\beta$, $\nu_\alpha$) from each $I = 1/2$ nucleus in the 2D spectrum. Powder HYSCORE spectra of $I = 1/2$ nuclei reveal, in the form of cross-ridges, the interdependence of $\nu_\alpha$ and $\nu_\beta$ in the same orientations (see Figure 1). The two coordinates of the arbitrary point at the cross-ridge, described in the first-order by the equation

$$\nu_{\alpha(\beta)} = |\nu_c + (-) A/2| \quad (2)$$

can be used for the first-order estimate of the corresponding hyperfine coupling constant A


dx.doi.org/10.1021/bi400489b | *Biochemistry* 2013, 52, 4648−4655

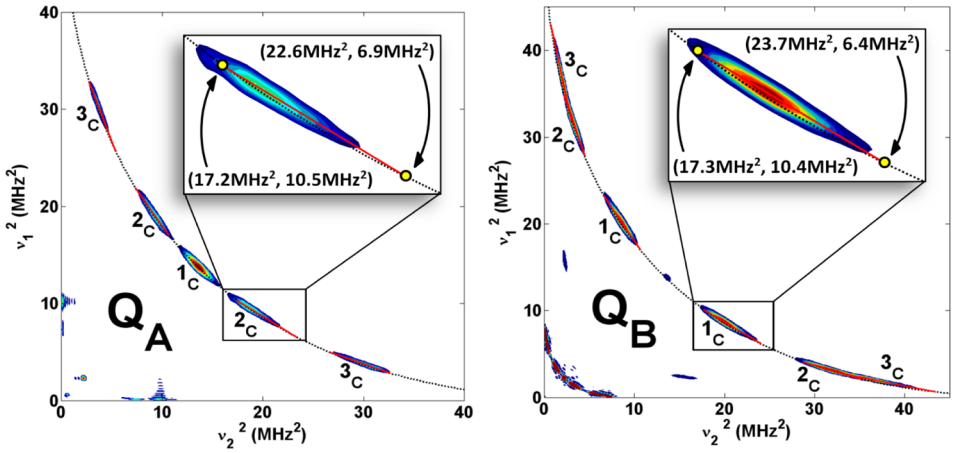


**Figure 2.** Contour presentation of the HYSCORE spectra of $SQ_A$ (left) and $SQ_B$ (right) in (Figure 1) in $((\nu_1)^2$ vs $(\nu_2)^2)$ coordinates. The dotted curve is defined by $|\nu_1 \pm \nu_2| = 2\nu_C$. Inserts show the linear regression fits for selected cross-peaks. (Graphs showing insets for the other fitted ridges are included in the Supporting Information.)

$$\nu_\alpha - \nu_\beta = A \tag{3}$$

Analysis of the ridges in $(\nu_\alpha)^2$ vs $(\nu_\beta)^2$ coordinates allows for direct, simultaneous determination of the isotropic $a$ and anisotropic $T$ components of the hyperfine tensor as described below in Results.[40,41]

## RESULTS

The $^{13}C$ hyperfine couplings in $SQ_A$ and $SQ_B$ were probed by HYSCORE experiments. Figure 1 shows representative HYSCORE spectra for $SQ_A$ and $SQ_B$ in the frequency interval from 0 to 7 MHz for both axes. The spectra of the SQ in both sites contain the lines from $^{15}N$ and $^{13}C$ nuclei. Here we focus on the analysis of the $^{13}C$ lines. The $^{13}C$ cross-features are located along the antidiagonal, symmetrically around the diagonal point $(\nu_C, \nu_C)$ where $\nu_C$ is ~3.7 MHz, in the applied magnetic field. The locations of the cross-peaks are significantly different for the two SQs.

The spectrum of $SQ_A$ (Figure 1) exhibits a peak $\mathbf{1}_C$ located around diagonal point $(\nu_C, \nu_C)$ and two pairs of cross-peaks $\mathbf{2}_C$ and $\mathbf{3}_C$. They are positioned symmetrically around the diagonal peak, along the antidiagonal, with maxima at (4.3, 3.1) MHz $(\mathbf{2}_C)$ and (5.5, 1.9) MHz $(\mathbf{3}_C)$, which correspond to first-order estimated hyperfine couplings 1.2 and 3.6 MHz, respectively. The width of these cross-ridges allows us to conclude that the dominant contributions to these couplings come from the isotropic constant. On the other hand, the line shape of the $\mathbf{1}_C$ peak suggests that the isotropic constant is close to zero in this case.

In contrast, the spectrum of $SQ_B$ (Figure 1) consists of three pairs of cross-peaks $\mathbf{1}_C - \mathbf{3}_C$. Cross-peaks $\mathbf{2}_C$ and $\mathbf{3}_C$ are partially overlapped, but their maxima are well separated. Coordinates of the maxima at (4.5, 3.0) MHz $(\mathbf{1}_C)$, (5.7, 1.7) MHz $(\mathbf{2}_C)$, and (6.0, 1.5) MHz $(\mathbf{3}_C)$ define the couplings 1.5, 4.0, and 4.5 MHz, respectively. The spectrum also contains a sharp peak of low intensity at the diagonal point $(\nu_C, \nu_C)$. We assign this line to weakly coupled, natural abundance (1.1%) $^{13}C$ nuclei present in the protein surrounding of $SQ_B$. In the $SQ_A$ spectrum a similar line is masked by the significantly more intense $\mathbf{1}_C$ diagonal feature from one site-specifically labeled carbon.

More complete information about separate values of the isotropic and anisotropic parts of hyperfine tensor of the $^{13}C$ nuclei contributing to the spectra of $SQ_A$ and $SQ_B$ can be obtained from the analysis of the contour line shape of the cross-peaks. The contour line shape of cross-peaks in the form of narrow ridges extending along the antidiagonal suggests an axial anisotropic hyperfine tensor for all contributing $^{13}C$. The analysis providing isotropic and anisotropic hyperfine couplings is straightforward in this case. The ideal cross-peak shape is an arc-type ridge between the points $(\nu_{\alpha\perp}, \nu_{\beta\perp})$ and $(\nu_{\alpha\parallel}, \nu_{\beta\parallel})$ located on the $|\nu_\alpha \pm \nu_\beta| = 2\nu_C$ lines. The shape of the ridge is described by the general equation $\nu_\alpha = (Q\nu_\beta^2 + G)^{1/2}$, where Q and G are coefficients that are functions of $a$, $T$, and $\nu_C$.[39,40] This line shape transforms into a straight line segment in the coordinates $(\nu_\alpha)^2$ vs $(\nu_\beta)^2$. It should be noted, however, that HYSCORE intensity at points $(\nu_{\alpha\perp}, \nu_{\beta\perp})$ and $(\nu_{\alpha\parallel}, \nu_{\beta\parallel})$, corresponding to orientations of the magnetic field along the $A_\perp$ and $A_\parallel$ principal directions of the hyperfine tensor, is equal to zero and is significantly suppressed in the orientations around the principal directions.[41] Therefore, in HYSCORE spectra, only the central part of the cross-ridge, which corresponds to orientations of the magnetic field substantially different from the principal directions, will possess observable intensity.[41] This means that in real spectra the cross-peak borders do not cross the $|\nu_1 \pm \nu_2| = 2\nu_C$ line(s). However, the crossing points $(\nu_{\alpha\perp}, \nu_{\beta\perp})$ and $(\nu_{\alpha\parallel}, \nu_{\beta\parallel})$ can be determined through the linear fitting of the observable parts in $(\nu_1)^2$ vs $(\nu_2)^2$ coordinates.[40,41]

Linear regression of the cross-peaks in the spectra of $SQ_A$ and $SQ_B$ plotted in the $(\nu_1)^2$ vs $(\nu_2)^2$ coordinates is shown in Figure 2. Linear regression gives intersection points with the $|\nu_1 \pm \nu_2| = 2\nu_C$ curve for each cross-peak. These points define two principal values of the hyperfine tensor. There are two possible assignments to $(\nu_{\alpha\perp}, \nu_{\beta\perp})$ or $(\nu_{\alpha\parallel}, \nu_{\beta\parallel})$ for each crossing point and, consequently, two solutions, one for each assignment. The tensors obtained from the analysis of the $SQ_A$ and $SQ_B$ spectra are summarized in Table 1. Uncertainty in assignment of $\nu_1$ to $\nu_\alpha$ or $\nu_\beta$ and, respectively, $\nu_2$ to $\nu_\beta$ or $\nu_\alpha$, allows alternate signs of $a$ and $T$ in both solutions (see footnote to Table 1). Complete information for the linear regression analysis of all cross-peaks and calculation of the tensors is provided in Supporting Information (Table S1 and Figure S2).

In order to choose between the two sets of axial tensors from analysis of $^{13}C$ HYSCORE plotted as $(\nu_1)^2$ vs $(\nu_2)^2$, the $^{13}C$ ridges for $Q_A$ and $Q_B$ were simulated with EasySpin.[35] For both


dx.doi.org/10.1021/bi400489b | Biochemistry 2013, 52, 4648−4655

**Table 1. $^{13}C$ Hyperfine Tensors for $SQ_A$ and $SQ_B$ from Linear Regression of Ridges Plotted as $(\nu_1)^2$ vs $(\nu_2)^2$[a]**

| Site | Set | $a$ (MHz) | $T$ (MHz) |
|---|---|---|---|
| $Q_A$ | $\mathbf{2}_C$ | 1.3(±0.2) | 0.4(±0.1) |
| | | −1.7(±0.2) | 0.4(±0.1) |
| | $\mathbf{3}_C$ | 3.2(±0.1) | 0.4(±0.1) |
| | | −3.6(±0.1) | 0.4(±0.1) |
| $Q_B$ | $\mathbf{1}_C$ | 1.4(±0.2) | 0.5(±0.1) |
| | | −1.9(±0.2) | 0.5(±0.1) |
| | $\mathbf{2}_C$ | 3.6(±0.1) | 0.4(±0.1) |
| | | −4.0(±0.1) | 0.4(±0.1) |
| | $\mathbf{3}_C$ | 4.6(±0.1) | 0.6(±0.1) |
| | | −5.2(±0.1) | 0.6(±0.1) |

[a]Signs of $a$ and $T$ are relative to the general form of two solutions: $(\pm a_1, \pm T)$ and $(\pm a_2, \mp T)$ with equal $|2a_1+T|$ and $|2a_2+T|$.

$Q_A$ and $Q_B$, simulated spectra were found to be essentially independent of the relative Euler angles between the $^{13}C$ hyperfine tensors, possibly due to the low level of hyperfine anisotropy. Thus, spectra for both solution sets for $a$ and $T$ from Table 1 were simulated and compared without adjusting the Euler angles.

For $SQ_A$, simulations with one set of axial tensors were in much better agreement with the experimental spectrum than the other. Peak $\mathbf{1}_C$ was simulated, and it was found that its isotropic coupling could not deviate from zero by more than 0.2 MHz for the line shape to resemble experimental data. For $SQ_B$, simulations with slightly rhombic tensors showed much better agreement with the experimental spectra for $\mathbf{1}_C$ and $\mathbf{3}_C$ features.

Preferred tensors revealed from the HYSCORE spectra simulations are shown in Table 2. Spectra simulated for two possible tensors for each cross-feature in $SQ_A$ and $SQ_B$ spectra and their comparative analysis are provided in Supporting Information (Table S2 and Figure S3).

**Table 2. $^{13}C$ Hyperfine Tensors Determined from the HYSCORE Spectra Simulations for $SQ_A$ and $SQ_B$**

| Site | Set | $a$ (MHz) | $T$ (MHz) |
|---|---|---|---|
| $Q_A$ | $\mathbf{1}_C$ | 0 | 0.4 |
| | $\mathbf{2}_C$ | 1.3 | 0.5 |
| | $\mathbf{3}_C$ | −3.6 | 0.4 |
| $Q_B$ | $\mathbf{1}_C$ | 1.5 | 0.4 ($\delta$=0.3) |
| | $\mathbf{2}_C$ | −3.9 | 0.4 |
| | $\mathbf{3}_C$ | 4.7 | 0.4 ($\delta$=0.1) |

## DISCUSSION

For the selectively $^{13}C$ labeled samples used here, three $^{13}C$ hyperfine couplings are expected corresponding to the two methoxy groups and the methyl group carbon nuclei. The HYSCORE spectra of Figures 1 and 2 clearly illustrate these three hyperfine couplings for both $SQ_A$ and $SQ_B$. Analysis of the spectra shows that for $SQ_A$ one of these carbons has a hyperfine coupling close to zero, whereas values of magnitude 1.2 and 3.6 MHz can be estimated for the other two. For $SQ_B$, values of magnitude 1.5, 4.0, and 4.5 MHz can be estimated. From the spectral lineshapes, low anisotropy is expected, with the estimated values dominated by the isotropic contribution. This is confirmed by a detailed line shape analysis and spectral simulations, which separate out the isotropic and anisotropic components, as shown in Tables 1 and 2. For the assignment of these measured values to the $^{13}C$ nuclei of the methyl or methoxy groups, it is necessary to compare with previous experimental results *in vitro* and with values calculated using DFT.

$^{13}C$ hyperfine couplings for the methyl group in ubisemiquinone and the related durosemiquinone (DQ) radicals have been previously reported in hydrogen bonding solvents (Table 3). For DQ an isotropic coupling of magnitude 3.8 MHz has been reported using ENDOR.[42,43] A similar coupling of around 4.0 MHz has been reported for the semiquinone anion radical of UQ-10 in alcohol solution.[44] Calculated DFT (B3LYP/EPR-II) hyperfine couplings for a hydrogen bonded DQ have been reported and the calculated negative isotropic constant of −3.5 MHz is in good agreement with the experimental magnitude.[45] These calculations also indicated that $a$ and $T$ have opposite signs in the $^{13}C$ methyl hyperfine tensor. In the current study we have also used $SQ_{M1}$ (6-methyl-UQ with 4 $H_2O$) to simulate the hydrogen bonded ubisemiquinone in solution. After geometry optimization the calculated C5′-methyl group $^{13}C$ isotropic coupling of −3.8 MHz is again in good agreement with the magnitude of the experimental finding, 4.0 MHz. Experimental and calculated values for the ubisemiquinone in the $SQ_H$ site from cytochrome $bo_3$ ubiquinol oxidase and its D75H mutant are also shown. The data in Table 3 indicate an impressive ability of DFT (B3LYP/EPR-II) to reproduce the experimental value of methyl coupling, though all calculated magnitudes are slightly less than the experimental determination.

**Table 3. Comparison of Experimental and Calculated $^{13}C$ Methyl (5′) Isotropic Constants in SQs**

| Semiquinone | $a_{exp}(^{13}C)$, MHz | $a_{calc}(^{13}C)$, MHz |
|---|---|---|
| UQ-10 | \|4.0\|[a] | −3.8 |
| DQ | \|3.8\|[b] | −3.5[c] |
| $SQ_H$ | −6.1[d] | −5.3[e] |
| $SQ_H$ (D75H) | −4.7[d] | −4.4[e] |
| $SQ_A$ | −3.6 | −2.9 |
| $SQ_B$ | −3.9 | −3.5 |

[a]ref 44. [b]refs 42, 43. [c]ref 45. [d]ref 27. [e]ref 46.

Table 3 also shows the DFT calculated $^{13}C$ isotropic couplings for the C5′-methyl group in the $SQ_A$ and $SQ_B$ site models. For $SQ_A$, therefore, we can confidently assign the pair $a$ = −3.6 MHz and $T$ = +0.4 MHz (Table 2, set $\mathbf{3}_C$) to the 5′ methyl group. The isotropic constants from the other two sets (∼0 and −1.7 MHz) are too small to be attributed to this group. For $SQ_B$ the calculated value of −3.5 MHz strongly suggests that the pair $a$ = −3.9 MHz and $T$ = +0.4 MHz (Table 2, set $\mathbf{2}_C$) corresponds to the methyl $^{13}C$. The other isotropic couplings of value |4.7| MHz and |1.5| MHz are too large and too small, respectively.

Based on the above analysis, the two remaining hyperfine tensors must correspond to the $^{13}C$ interaction for the two methoxy groups. In this case analysis is complicated by the expected dependency of the tensor on the orientation of the methoxy group relative to the ring plane. To aid assignment it is first instructive to examine the Mülliken spin populations calculated for each semiquinone and these are given in Table 4.

For $SQ_A$, values of +0.11 and −0.01 are calculated for positions at C2 and C3, respectively. This arises from the polarization of the spin density distribution caused by the


dx.doi.org/10.1021/bi400489b | *Biochemistry* 2013, 52, 4648−4655

**Table 4. Mülliken Spin Populations in Selected SQs**

| Semiquinone | C2 | C3 |
|---|---|---|
| $SQ_A$ | 0.11 | −0.01 |
| $SQ_B$ | 0.09 | 0.02 |
| $SQ_{M2}$ | 0.11 | 0.00 |
| $SQ_{M1}$ | 0.07 | 0.07 |

stronger hydrogen bonding to the O1 oxygen atom, as discussed previously.[38]

The $^{13}C$ isotropic hyperfine coupling of the methoxy group will be proportional to the $\pi(p)$ spin population of the corresponding ring carbon and the dihedral angle of the methoxy CO bond with respect to the SQ ring plane; see below. Based on the near zero calculated spin population for the C3 position, the diagonal peak $\mathbf{1}_C$ with isotropic coupling close to zero is expected for the 3-methoxy group carbon. The remaining cross-peaks $\mathbf{2}_C$ and corresponding $^{13}C$ coupling with magnitude 1.3 MHz therefore can only arise from the 2-methoxy carbon.

For $SQ_B$, Table 4 shows that, as for $SQ_A$, the calculated spin population at position C2 (0.09) is again substantially larger than C3 (0.02). Based on this we expect that the 2-methoxy $^{13}C$ isotropic hyperfine coupling is significantly larger than the 3-methoxy $^{13}C$ value. Thus, from Figure 2 and Table 2, we can assign the larger magnitude 4.7 MHz coupling to the C2 methoxy carbon and the smaller one of magnitude 1.5 MHz to the C3 methoxy. Therefore, the optimized simulation data in Table 2 and DFT calculations (Tables 3 and 4) allows us to make fully consistent assignments of $^{13}C$ hyperfine tensors determined for $SQ_A$ and $SQ_B$ to particular substituents.

The assignments above suggest that the 2-methoxy $^{13}C$ isotropic constant is significantly larger for $SQ_B$ compared with $SQ_A$. This cannot be explained on the basis of the C2 spin population value, which is larger (0.11 versus 0.09) for the $SQ_A$. The unpaired spin density giving rise to the $^{13}C$ isotropic hyperfine coupling for the methoxy group carbon atom arises from a combination of spin polarization and hyperconjugation. When the methoxy group is held in the ring plane, hyperconjugation is expected to be zero and small negative hyperfine couplings are expected for in or near in-plane orientations, due to spin polarization by the methoxy oxygen spin density. As the methoxy orientation is moved progressively out of plane a positive contribution arising from hyperconjugation with the ring carbon $\pi(p)$ spin density arises. For the $SQ_{M2}$ model (6-methyl-UQ with 1 $H_2O$), which approximates the asymmetric hydrogen bonding of $SQ_A$ and $SQ_B$, Figure 3 shows that the isotropic coupling exhibits this trend with negative values at in-plane orientations and large positive values for out of plane orientations. The $SQ_{M2}$ model spin populations at C2 and C3 are very similar to the $SQ_A$ values (Table 4). The $^{13}C$ data obtained for $SQ_B$ compared with $SQ_A$ implies that the 2-methoxy group is oriented further out of the ring plane thereby giving rise to the larger isotropic coupling.

Figure 3 allows us to estimate the difference in 2-methoxy conformation in $SQ_A$ and $SQ_B$. An isotropic coupling of 1.3 MHz corresponds to a 2-methoxy conformation of ∼50° or ∼155°. In contrast, the simulated isotropic coupling for 2-methoxy in $SQ_B$, adjusted to the C2 spin population 0.11, as in the $SQ_{M2}$ model, is 5.6 MHz, i.e., multiplied by 1.22, and defines the conformation as ∼75° or ∼135°. These estimates

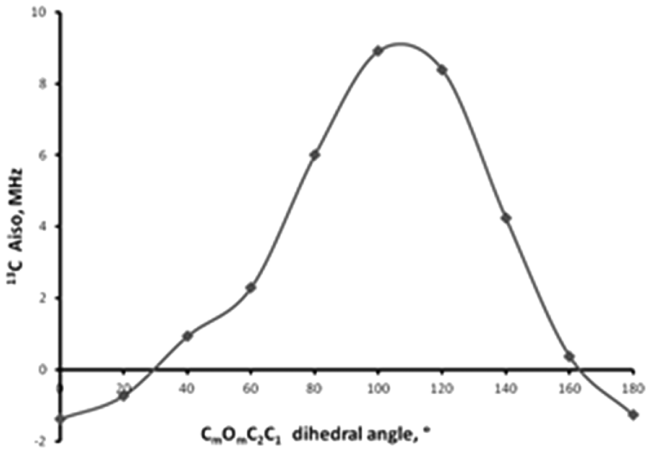


**Figure 3.** Effect of rotation of the 2-methoxy group on its $^{13}C$ isotropic hyperfine constant for model $SQ_{M2}$.

indicate a difference on the order of ∼20−25° between the 2-methoxy conformations in $SQ_A$ and $SQ_B$.

DFT calculations on the hydrogen bonded ubisemiquinone model $SQ_{M2}$ also show that the electron affinity of the quinone increases as the methoxy group is rotated out of the ring plane (Figure 4). The more out of plane orientation exhibited by the

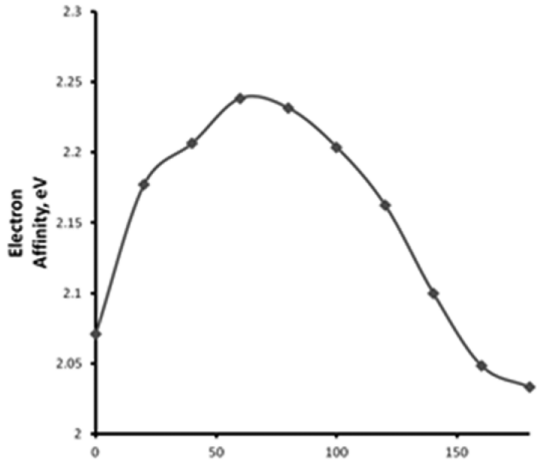


**Figure 4.** Effect of rotation of the 2-methoxy dihedral angle in steps of 20° on the electron affinity of model $SQ_{M2}$.

2-methoxy group in $SQ_B$ suggests a greater electron affinity value for $Q_B$ which should lead to a higher redox potential compared with $Q_A$. Our estimated difference of the 2-methoxy conformation of ∼20−25° corresponds to $\Delta E_A$ ∼0.05 eV giving a predicted 50 mV difference in redox potential between $Q_A$ and $Q_B$. This is a significant fraction of the experimental difference, $\Delta E_m$ = 60−75 mV, indicating that the orientation of the 2-methoxy group between $Q_A$ and $Q_B$ may be a crucial factor in determining the functional $E_m$ drop between $Q_A$ and $Q_B$. Further studies aimed at providing a more quantitative measure of this factor in governing the redox potential of $Q_A$ and $Q_B$ are in progress.

## ■ CONCLUSIONS

HYSCORE studies on bacterial reaction centers, with $Q_A$ and $Q_B$ site ubiquinones $^{13}C$-labeled at the headgroup methyl and methoxy groups, have been performed. $^{13}C$ isotropic and anisotropic hyperfine couplings have been obtained and are


dx.doi.org/10.1021/bi400489b | *Biochemistry* 2013, 52, 4648−4655

compared to those calculated by density functional theory. This has allowed firm assignment of measured hyperfine tensors to specific methyl and methoxy carbon nuclei. Further computational analysis indicates a difference in the conformation of the 2-methoxy group between the $Q_A$ and $Q_B$ site semiquinone forms. This difference is attributed to a more out of plane orientation of the 2-methoxy group adopted by the $Q_B$ semiquinone. An out of plane orientation is also shown to be associated with increased electron affinity, indicating that it can contribute significantly to the higher redox potential of the $Q_B$ site ubiquinone in bacterial type II reaction centers. This work shows that $^{13}C$ HYSCORE, coupled with high quality DFT calculations, provide a very sensitive method for characterizing methoxy group orientations in ubisemiquinone, as manifested in the changes of the $^{13}C$ isotropic hyperfine couplings. Preliminary results obtained for other systems indicate that this approach, with appropriate development of the theoretical foundations, will allow quantitative measures for the redox potentials of ubiquinone in other quinone processing sites in proteins.

## ■ ASSOCIATED CONTENT

### Supporting Information

Figures S1 − S3, Tables S1 and S2. This material is available free of charge via the Internet at http://pubs.acs.org.

## ■ AUTHOR INFORMATION


### Corresponding Author

*S.A.D.: e-mail, dikanov@illinois.edu; phone, (217) 300-2209. C.A.W.: e-mail: cwraight@life.illinois.edu; phone, (217) 333-3245. P.J.O.: e-mail: patrick.omalley@manchester.ac.uk; phone, 00441612004536.


### Author Contributions

The manuscript was written through contributions of all authors. All authors have given approval to the final version of the manuscript


### Funding Statement

This research was supported by the DE-FG02-08ER15960 Grant from Chemical Sciences, Geosciences and Biosciences Division, Office of Basic Energy Sciences, Office of Sciences, US DOE and NIH Grant GM062954 (S.A.D.), NSF Grant MCB-0818121 (C.A.W.) and NCRR/NIH Grant S10-RR15878 and S10-RR025438 for pulsed EPR instrumentation. PJOM acknowledges the use of computer resources granted by the EPSRC UK national service for computational chemistry software (NSCCS). A.T.T. gratefully acknowledges support as a NIH trainee of the Molecular Biophysics Training Program (5T32-GM008276).


### Notes

The authors declare no competing financial interest.

## ■ ACKNOWLEDGMENTS


The authors gratefully acknowledge Dr. Myat Lin and Prof. R. B. Gennis for the auxotrophic *E. coli* strain and Dr. A. Baldansuren for help during the pulsed EPR experiments at the early stage of this work.


## ■ ABBREVIATIONS

2D, two-dimensional; CW, continuous-wave; DFT, density functional theory; B3LYP, Becke3 Lee−Yang−Parr; SQ, semiquinone; RC, reaction center; EPR, electron paramagnetic resonance; ENDOR, electron nuclear double-resonance; ESEEM, electron spin echo envelope modulation; HYSCORE, hyperfine sublevel correlation; UQ-10, ubiquinone-10

## ■ REFERENCES


(1) Heathcote, P., Fyfe, P. K., and Jones, M. R. (2002) Reaction centers: the structure and evolution of biological solar power. *Trends Biochem. Sci. 27*, 79−86.

(2) Blankenship, R. (2002) *Molecular mechanisms of photosynthesis*, Blackwell Science, Ltd, London.

(3) Wraight, C. A. (2004) Proton and electron transfer in the acceptor quinone complex of photosynthetic reaction centers from *Rhodobacter sphaeroides*. *Front. Biosci. 9*, 309−337.

(4) Wraight, C. A., and Gunner, M. R. (2009) The Acceptor Quinones of Purple Photosynthetic Bacteria—Structure and Spectroscopy. *The Purple Phototrophic Bacteria* (Hunter, C. N., Daldal, F., Thurnauer, M. C., and Beatty, J. T., Eds.) pp 379, Springer Science + Business Media B.V..

(5) Wraight, C. A. (1979) Electron acceptors of bacterial photosynthetic reaction centers II. $H^+$ binding coupled to secondary electron transfer in the quinone acceptor complex. *Biochim. Biophys. Acta 548*, 309−327.

(6) Blankenship, R. E., and Parson, W. W. (1979) The involvement of iron and ubiquinone in electron transfer reactions mediated by reaction centers from photosynthetic bacteria. *Biochim. Biophys. Acta 545*, 429−444.

(7) Kleinfeld, D., Okamura, M. Y., and Feher, G. (1984) Electron transfer in reaction centers of *Rhodopseudomonas sphaeroides*: I. Determination of the charge recombination pathway of $D+Q_AQ_B^-$ and free energy and kinetic relations between $Q_A^-$ $Q_B$ and $Q_AQ_B^-$. *Biochim. Biophys. Acta 766*, 126−140.

(8) Mancino, L. J., Dean, D. P., and Blankenship, R. E. (1984) Kinetics and thermodynamics of the $P870^+Q_A^- \rightarrow P870^+Q_B^-$ reaction in isolated reaction centers from the photosynthetic bacterium *Rhodopseudomonas sphaeroides*. *Biochim. Biophys. Acta 764*, 46−54.

(9) Shinkarev, V. P., and Wraight, C. A. (1997) The interaction of quinone and detergent with reaction centers of purple bacteria. I. Slow quinone exchange between reaction center micelles and pure detergent micelles. *Biophys. J. 72*, 2304−2319.

(10) Wraight, C. A., Vakkasoglu, A. S., Poluektov, Y., Mattis, A. J., Nihan, D., and Lipshutz, B. H. (2008) The 2-methoxy group of ubiquinone is essential for function of the acceptor quinones in reaction centers from *Rba. sphaeroides*. *Biochim. Biophys. Acta 1777*, 631−636.

(11) McComb, J. C., Stein, R. R., and Wraight, C. A. (1990) Investigations on the influence of headgroup substitution and isoprene side-chain length in the function of primary and secondary quinones of bacterial reaction centers. *Biochim. Biophys. Acta 1015*, 156−171.

(12) Prince, R. C., Dutton, P. L., and Bruce, J. M. (1983) Electrochemistry of ubiquinones, menaquinones and plastoquinones in aprotic solvents. *FEBS Lett. 160*, 273−276.

(13) Gu, L. Q., Yu, L., and Yu, C. A. (1990) Effect of substituents of the benzoquinone ring on electron-transfer activities of ubiquinone derivatives. *Biochim. Biophys. Acta 1015*, 482−492.

(14) Nabedryk, E., and Breton, J. (2008) Coupling of electron transfer to proton uptake at the Q(B) site of the bacterial reaction center: a perspective from FTIR difference spectroscopy. *Biochim. Biophys. Acta 1777*, 1229−1248.

(15) Lubitz, W., and Feher, G. (1999) The Primary and Secondary Acceptors in Bacterial Photosynthesis III. Characterization of the Quinone Radicals $Q_A^-$ and $Q_B^-$ by EPR and ENDOR. *Appl. Magn. Reson. 17*, 1−48.

(16) Dikanov, S. A. (2013) Resolving protein-semiquinone interactions by two-dimensional ESEEM spectroscopy. *Electron Paramagn. Resonan. 23*, 103−179.

(17) Breton, J., and Nabedryk, E. (1996) Protein-quinone interactions in the bacterial photosynthetic reaction center: Light-

induced FTIR difference spectroscopy of the quinone vibrations. *Biochim. Biophys. Acta 1275*, 84−90.
(18) Nonella, M., and Brändli, C. (1996) Density functional investigation of methoxy-substituted *p*-benzoquinones: Conformational analysis and harmonic force fields of 2-methoxy- and 2,3-dimethoxy-1,4-benzoquinone. *J. Phys. Chem. 100*, 14549−14559.
(19) Burie, J.-R., Boullais, C., Nonella, M., Mioskowski, C., Nabedryk, E., and Breton, J. (1997) Importance of the conformation of methoxy groups on the vibrational and electrochemical properties of ubiquinones. *J. Phys. Chem. B 101*, 6607−6617.
(20) Nonella, M. (1997) Structure and vibrational spectra of *p*-benzoquinone in different oxidation and protonation states: A density functional study. *J. Phys. Chem. B 101*, 1235−1246.
(21) Nonella, M. (1998) A quantum chemical investigation of structures, vibrational spectra and electron affinities of the radicals of quinone model compounds. *Photosynth. Res. 55*, 253−259.
(22) Nonella, M., Mathias, G., Eichinger, M., and Tavan, P. (2003) Structures and vibrational frequencies of the quinones of *Rb. sphaeroides* derived by a combined density functional/molecular mechanics approach. *J. Phys. Chem. B 107*, 316−322.
(23) Boullais, C., Nabedryk, E., Burie, J.-R., Nonella, M., Mioskowski, C., and Breton, J. (1998) Site-specific isotope labeling demonstrates a large mesomeric resonance effect of the methoxy groups on the carbonyl frequency in ubiquinones. *Photosynth. Res. 55*, 247−252.
(24) Breen, D. L. (1975) Coenzyme Q: A molecular orbital study. *J. Theor. Biol. 53*, 101−113.
(25) Robinson, H., and Kahn, S. (1990) Interplay of substitutent conformation and electron affinity in quinone models of quinone reductases. *J. Am. Chem. Soc. 112*, 4728−4731.
(26) Prince, R. C., Halbert, T. R., and Upton, T. H. (1988) Structural influences on the electrochemistry of ubiquinone. *Advances in Membrane Biochemistry and Bioenergetics* (Kim, C. H., Tedeschi, H., Diwan, J. J., Salerno, J. C., Eds.) pp 469−478, Plenum Press, New York.
(27) Remy, A., Boers, R. B., Egorova-Zachernyuk, T., Gast, P., Lugtenburg, J., and Gerwert, K. (2003) Does different orientation of the methoxy groups of ubiquinone-10 in the reaction center of *Rhodobacter sphaeroides* cause different binding at $Q_A$ and $Q_B$? *Eur. J. Biochem. 270*, 3603−3609.
(28) Lin, M. T., Shubin, A. A., Samoilova, R. I., Narasimhulu, K. V., Baldansuren, A., Gennis, R. B., and Dikanov, S. A. (2011) Exploring by pulsed EPR the electronic structure of ubisemiquinone bound at the $Q_H$ site of cytochrome $bo_3$ from *Escherichia coli* with *in vivo* $^{13}$C-labeled methyl and methoxy substituents. *J. Biol. Chem. 286*, 10105−10114.
(29) Lin, M. T., Sperling, L. J., Frericks Schmidt, H. L., Tang, M., Samoilova, R. I., Kumasaka, T., Iwasaki, T., Dikanov, S. A., Rienstra, Ch. M., and Gennis, R. B. (2011) A rapid and robust method for selective isotope labeling of proteins. *Methods 55*, 370−378.
(30) Goldsmith, J. O., and Boxer, S. G. (1996) Rapid isolation of bacterial photosynthetic reaction center with an engineered polyhistidine tag. *Biochim. Biophys. Acta 1276*, 171−175.
(31) Stoll, S., Calle, C., Mitrikas, G., and Schweiger, A. (2005) Peak suppression in ESEEM spectra of multinuclear spin systems. *J. Magn. Reson. 177*, 93−101.
(32) Martin, E., Samoilova, R .I., Narasimhulu, K. V., Wraight, C. A., and Dikanov, S. A. (2010) Hydrogen bonds between nitrogen donors and the semiquinone in the $Q_B$-site of bacterial reaction centers. *J. Am. Chem. Soc. 132*, 11671−11677.
(33) Okamura, M., Isaacson, R., and Feher, G. (1975) Primary acceptor in Bacterial Photosynthesis: Obligatory role of Ubiquinone in Photoactive Reaction Centers of *Rhodopseudomonas spheroides*. *Proc. Nat. Acad. Sci. U.S.A. 72*, 3491−3495.
(34) Höfer, P., Grupp, A., Nebenführ, H., and Mehring, M. (1986) Hyperfine sublevel correlation (HYSCORE) spectrocopy: A 2D ESR investigation of the squaric acid radical. *Chem. Phys. Lett. 132*, 279−282.
(35) Stoll, S., and Britt, R. D. (2009) General and efficient simulation of pulse EPR spectra. *Phys. Chem. Chem. Phys. 11*, 6614−6625.
(36) Frisch, M. J., Trucks, G. W., Schlegel, H. B., Scuseria, G. E., Robb, M. A., Cheeseman, J. R., Scalmani, G., Barone, V., Mennucci, B., Petersson, G. A., Nakatsuji, H., Caricato, M., Li, X., Hratchian, H. P., Izmaylov, A. F., Bloino, J., Zheng, G., Sonnenberg, J. L., Hada, M., Ehara, M., Toyota, K., Fukuda, R., Hasegawa, J., Ishida, M., Nakajima, T., Honda, Y., Kitao, O., Nakai, H., Vreven, T., Montgomery, J. A., Jr., Peralta, J. E., Ogliaro, F., Bearpark, M., Heyd, J. J., Brothers, E., Kudin, K. N., Staroverov, V. N., Kobayashi, R., Normand, J., Raghavachari, K.,Rendell, A., Burant, J. C., Iyengar, S. S., Tomasi, J., Cossi, M., Rega, N., Millam, J. M., Klene, M., Knox, J. E., Cross, J. B., Bakken, V., Adamo, C., Jaramillo, J., Gomperts, R., Stratmann, R. E., Yazyev, O., Austin, A. J., Cammi, R., Pomelli, C., Ochterski, J. W., Martin, R. L., Morokuma, K., Zakrzewski, V. G., Voth, G. A., Salvador, P., Dannenberg, J. J., Dapprich, S., Daniels, A. D., Farkas, Ö, Foresman, J. B., Ortiz, J. V., Cioslowski, J., and Fox, D. J. (2009) Gaussian 09, revision A.1, Gaussian, Inc., Wallingford, CT.
(37) Lin, T.-J., and O'Malley, P. J. (2008) An ONIOM study of the QA site semiquinone in the *Rhodobacter sphaeroides* photosynthetic reaction centre. *J. Mol. Struct.: THEOCHEM 870*, 31−35.
(38) Martin, E., Samoilova, R. I., Narasimhulu, K. V., Lin, T. J., O'Malley, P. J., Wraight, C. A., and Dikanov, S. A. (2011) Hydrogen Bonding and Spin Density Distribution in the $Q_B$ Semiquinone of Bacterial Reaction Centers and Comparison with the $Q_A$ Site. *J. Am. Chem. Soc. 133*, 5525−5537.
(39) Martin, E., Baldansuren, A., Lin, T.-J., Samoilova, R. I., Wraight, C. A., Dikanov, S. A., and O'Malley, P. J. (2012) Hydrogen Bonding between the $Q_B$ Site Ubisemiquinone and Ser-L223 in the Bacterial Reaction Center: A Combined Spectroscopic and Computational Perspective. *Biochemistry 51*, 9086−9093.
(40) Dikanov, S. A., and Bowman, M. K. (1995) Cross-peak lineshape of two-dimensional ESEEM spectra in disordered S=1/2, I=1/2 spin system. *J. Magn. Reson., Ser. A 116*, 125−128.
(41) Dikanov, S. A., Tyryshkin, A. M., and Bowman, M. K. (2000) Intensity of cross-peaks in HYSCORE spectra of S=1/2, I=1/2 spin systems. *J. Magn. Reson. 144*, 228−242.
(42) Das, M. R., Connor, H. D., Leniart, D. S., and Freed, J. H. (1970) An Electron Nuclear Double Resonance and Electron Spin Resonance Study of Semiquinones Related to Vitamins K and E. *J. Am. Chem. Soc. 92*, 2258−2268.
(43) Kirste, B. (1987) ENDOR studies of semiquinone radical ions in liquid crystalline solutions. *Magn. Reson. Chem. 25*, 166−175.
(44) Samoilova, R. I., Gritsan, N. P., Hoff, A. J., van Liemt, W. B. S., Lugtenburg, J., Spoyalov, A. P., and Tsvetkov, Yu. D. (1995) ENDOR and EPR studies of highly isotopically $^{13}$C-enriched ubiquinone radicals. Part 2. *J. Chem. Soc., Perkin. Trans. 2*, 2063−2068.
(45) O'Malley, P. J. (1998) B3LYP, Hybrid Density Functional Studies of the Durosemiquinone Radical: The Effect of Symmetrical and Asymmetrical Hydrogen Bonding on Spin Densities and Hyperfine Couplings. *J. Phys. Chem. A 102*, 248−253.
(46) Lin, M. T., Baldansuren, A., Hart, R., Samoilova, R. I., Narasimhulu, K. V., Yap, L.-L., Choi, S. K., O'Malley, P. J., Gennis, R. B., and Dikanov, S. A. (2012) Interactions of intermediate semiquinone with surrounding protein residues at the $Q_H$ site of the wild-type and D75H mutant cytochrome $bo_3$ from *Escherichia coli*. *Biochemistry 51*, 3827−3838.